

PAPER

# Initial results from boron powder injection experiments in WEST lower single null L-mode plasmas

To cite this article: G. Bodner *et al* 2022 *Nucl. Fusion* **62** 086020

View the [article online](#) for updates and enhancements.

## You may also like

- [Real-time wall conditioning and recycling modification utilizing boron and boron nitride powder injections into the Large Helical Device](#)  
R. Lunsford, S. Masuzaki, F. Nespoli et al.
- [MASTER OPTICAL POLARIZATION VARIABILITY DETECTION IN THE MICROQUASAR V404 CYG/GS 2023+33](#)  
Vladimir M. Lipunov, E. Gorbovskoy, V. Kornilov et al.
- [Overview of the emissivity measurements performed in WEST: \*in situ\* and post-mortem observations](#)  
J. Gaspar, Y. Corre, F. Rigollet et al.

# Initial results from boron powder injection experiments in WEST lower single null L-mode plasmas

G. Bodner<sup>1,\*</sup>, A. Gallo<sup>2</sup>, A. Diallo<sup>1</sup>, R. Lunsford<sup>1</sup>, Ph. Moreau<sup>2</sup>,  
A. Nagy<sup>1</sup>, F.-P. Pellissier<sup>2</sup>, C. Guillemaut<sup>2</sup>, J.P. Gunn<sup>2</sup>, C. Bourdelle<sup>2</sup>,  
C. Desgranges<sup>2</sup>, P. Manas<sup>2</sup>, A. Bortolon<sup>1</sup>, C.C. Klepper<sup>3</sup>, E. Tsitrone<sup>2</sup>,  
E.A. Unterberg<sup>3</sup>, L. Vermare<sup>4</sup> and the WEST Team<sup>a</sup>

<sup>1</sup> Princeton Plasma Physics Laboratory, Princeton, NJ, United States of America

<sup>2</sup> CEA, IRFM, F-13108 Saint-Paul-Lez-Durance, France

<sup>3</sup> Oak Ridge National Laboratory, Oak Ridge, TN, United States of America

<sup>4</sup> École Polytechnique—LPP, Paris, France

E-mail: [gbodner@pppl.gov](mailto:gbodner@pppl.gov)

Received 4 February 2022, revised 10 May 2022

Accepted for publication 18 May 2022

Published 15 June 2022



## Abstract

Using a recently installed impurity powder dropper (IPD), boron powder ( $<150\text{ }\mu\text{m}$ ) was injected into lower single null (LSN) L-mode discharges in WEST. IPDs possibly enable real-time wall conditioning of the plasma-facing components and may help to facilitate H-mode access in the full-tungsten environment of WEST. The discharges in this experiment featured  $I_p = 0.5\text{ MA}$ ,  $B_T = 3.7\text{ T}$ ,  $q_{95} = 4.3$ ,  $t_{\text{pulse}} = 12\text{--}30\text{ s}$ ,  $n_{e,0} \sim 4 \times 10^{19}\text{ m}^{-2}$ , and  $P_{\text{LHCD}} \sim 4.5\text{ MW}$ . Estimates of the deuterium and impurity particle fluxes, derived from a combination of visible spectroscopy measurements and their corresponding S/XB coefficients, showed decreases of  $\sim 50\%$  in  $\text{O}^+$ ,  $\text{N}^+$ , and  $\text{C}^+$  populations during powder injection and a moderate reduction of these low- $Z$  impurities ( $\sim 50\%$ ) and W ( $\sim 10\%$ ) in the discharges that followed powder injection. Along with the improved wall conditions, WEST discharges with B powder injection observed improved confinement, as the stored energy  $W_{\text{MHD}}$ , neutron rate, and electron temperature  $T_e$  increased significantly (10%–25% for  $W_{\text{MHD}}$  and 60%–200% for the neutron rate) at constant input power. These increases in confinement scale up with the powder drop rate and are likely due to the suppression of ion temperature gradient (ITG) turbulence from changes in  $Z_{\text{eff}}$  and/or modifications to the electron density profile.

Keywords: wall conditioning, powder injection, boronization, tungsten, impurity injection

(Some figures may appear in colour only in the online journal)

## 1. Introduction

Proper conditioning of the vacuum vessel walls is essential for the reliable operation of magnetic fusion devices [1]. In tokamaks and stellarators, the walls can serve as an unpredictable fueling source due to the outgassing of previously

trapped hydrogenic particles and as a potential impurity source due to physical and/or chemical sputtering. Tungsten (W) is the chosen first-wall material for the ITER divertor and is a prime candidate for the first wall material in a fusion pilon plant due to its low tritium (T) retention, high melting point, and high thermal conductivity. Unlike low- $Z$  elements, which are easily stripped of their electrons by the high temperature plasma, W continues to radiate as it penetrates deeper into the core hence reducing the plasma temperature. The sputtering of high- $Z$  particles into the plasma core has been shown to

\* Author to whom any correspondence should be addressed.

<sup>a</sup> The WEST Team (<https://west.cea.fr/WESTteam>).

decrease energy confinement in several tokamaks with high-Z plasma-facing components (PFCs) [2–4].

To investigate the impact of a high-Z first wall environment on high performance long-pulse discharges, Tore Supra has been converted into WEST (W Environment in Steady-state Tokamak). This upgrade consisted primarily of changing the plasma configuration from limited to diverted and changing the first-wall material from carbon (C) to tungsten [5, 6]. For the most recent C5 campaign, several actively-cooled ITER-like plasma facing units or PFUs (modelled after the ITER divertor vertical target) have been installed in the lower divertor of WEST to assess the viability of the monoblock divertor design [7] against ITER relevant heat fluxes (up to  $20 \text{ MW m}^{-2}$ ). Starting in 2022, WEST will feature a lower divertor composed of entirely actively-cooled ITER-like PFUs.

The transition from a carbon environment to a metallic environment has severe consequences for plasma performance; namely an increase in impurity radiation due to the influx of high-Z particles. To combat this, regular conditioning of the high-Z vacuum vessel walls is needed. One of the most common and effective methods of wall conditioning is glow discharge boronization (GDB), where thin layers of boron (B) are deposited onto the vacuum vessel walls to suppress wall fueling and impurity sputtering [8]. While boronization may not be desirable for a fusion pilot plant due to the T retention of the B films, it remains a valuable tool to expand the operational windows of present day tokamaks and stellarators. Boronization has been especially important to achieve high density regimes in WEST [9] and to suppress the sputtering of high-Z particles in other metal-walled tokamaks [10, 11].

Unfortunately, the standard procedure for GDB is not conducive to a superconducting fusion experiment like WEST or a steady-state pilot plant. Most GDB systems utilize toxic diborane gas ( $\text{B}_2\text{H}_6$  or  $\text{B}_2\text{D}_6$ ) and all require the de-energization of the magnetic field coils. These issues represent both a significant safety concern and a large time cost. In the case of superconducting experiments, this may be prohibitive as the coils only have a finite number of charge cycles. Therefore, a wall conditioning method that can be run in the presence of a strong magnetic field is highly desired. To address these concerns, the Princeton Plasma Physics Laboratory has developed the impurity powder dropper (IPD) [12].

IPDs are compact devices that can drop a multitude of low-Z powders (Li, B, C,  $\text{B}_4\text{C}$ , and BN) at reproducible drop rates into high temperature plasmas. The low-Z powder is ablated by the plasma and then deposited onto the PFCs through plasma-enhanced chemical vapor deposition. In addition to wall conditioning, IPDs can be used for impurity transport experiments and as a localized edge radiation mechanism, similar to gaseous impurity injection [13]. An in-depth technical overview of the IPD is given in [12]. Typical IPD operation drops powder at continuous rates of  $5\text{--}100 \text{ mg s}^{-1}$  or periodic  $\sim 10 \text{ mg s}^{-1}$  bursts into auxiliary heated discharges.

In the case of boronization, B, BN, and even  $\text{B}_4\text{C}$  powder are used. Boronization through powder injection has the benefit of using essentially pure boron powders as opposed to standard boronated gases ( $\text{B}_2\text{H}_6$ ,  $\text{B}_2\text{D}_6$ , and  $\text{B}_{10}\text{H}_{14}$ ), which

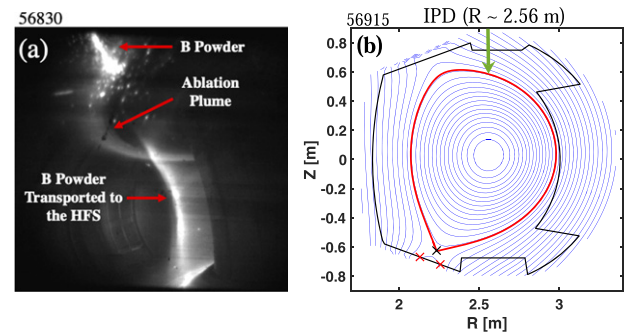


**Figure 1.** (a) Visible camera image of B powder being dropped into and ablated by a WEST discharge. (b) Representative equilibrium from the WEST IPD experimental campaign and IPD location.

introduce non-trivial quantities of hydrogenic species into the vessel. The major disadvantage of powder injection is that the deposition of the B atoms is subject to the magnetic field lines and plasma flows. Therefore, the deposition rate and coating homogeneity through the vessel are likely different and less extensive than that of standard GDB.

In January 2021, an IPD was installed on WEST to aid in the conditioning of the full-W environment and test the viability of the IPD at reactor-relevant time scales. While IPDs have previously been installed and operated on other metal-walled tokamaks such as AUG [14, 15] and EAST [16, 17], the long pulse capabilities and full-W environment make WEST an excellent test bed to extend the evaluation of the IPD as a real-time wall conditioning technique. The present results can additionally be compared with powder injection experiments in carbon-walled machines, namely DIII-D [18], KSTAR [19], W7-X [20], and LHD [21, 22].

This paper presents the first results of B powder injection in WEST L-Mode plasmas. Section 2 provides an overview of the first IPD experiments on WEST and shows the impact of B powder injection on key global plasma parameters. Section 3 presents evidence of improved wall conditioning both during and after B powder injection. Section 4 details observations of improved confinement during B powder injection discharges and its consequences for future IPD operation. Lastly, section 5 concludes this paper with a summary of the results.

## 2. IPD experiments on WEST

To prepare for the dedicated IPD experimental runs in 2022, an initial commissioning campaign was carried out in early 2021. Using the IPD, B powder (spherical shape with diameter  $< 150 \mu\text{m}$ ) was successfully dropped into 10 lower-single null (LSN) L-mode deuterium plasmas in WEST. These discharges featured plasma current  $I_p = 0.5 \text{ MA}$ , toroidal field  $B_T = 3.7 \text{ T}$ , lower hybrid current drive (LHCD) power  $P_{\text{LHCD}} \sim 4.5 \text{ MW}$ , edge safety factor  $q_{95} = 4.3$ , and volume-averaged electron density  $n_e \sim 3.5 \times 10^{19} \text{ m}^{-3}$  (Greenwald density fraction  $n_g = 0.45$ ). An image during the B powder drop from a visible camera is shown in figure 1(a) and a representative equilibrium with the IPD location is shown in figure 1(b). The B powder was clearly ablated by the plasma

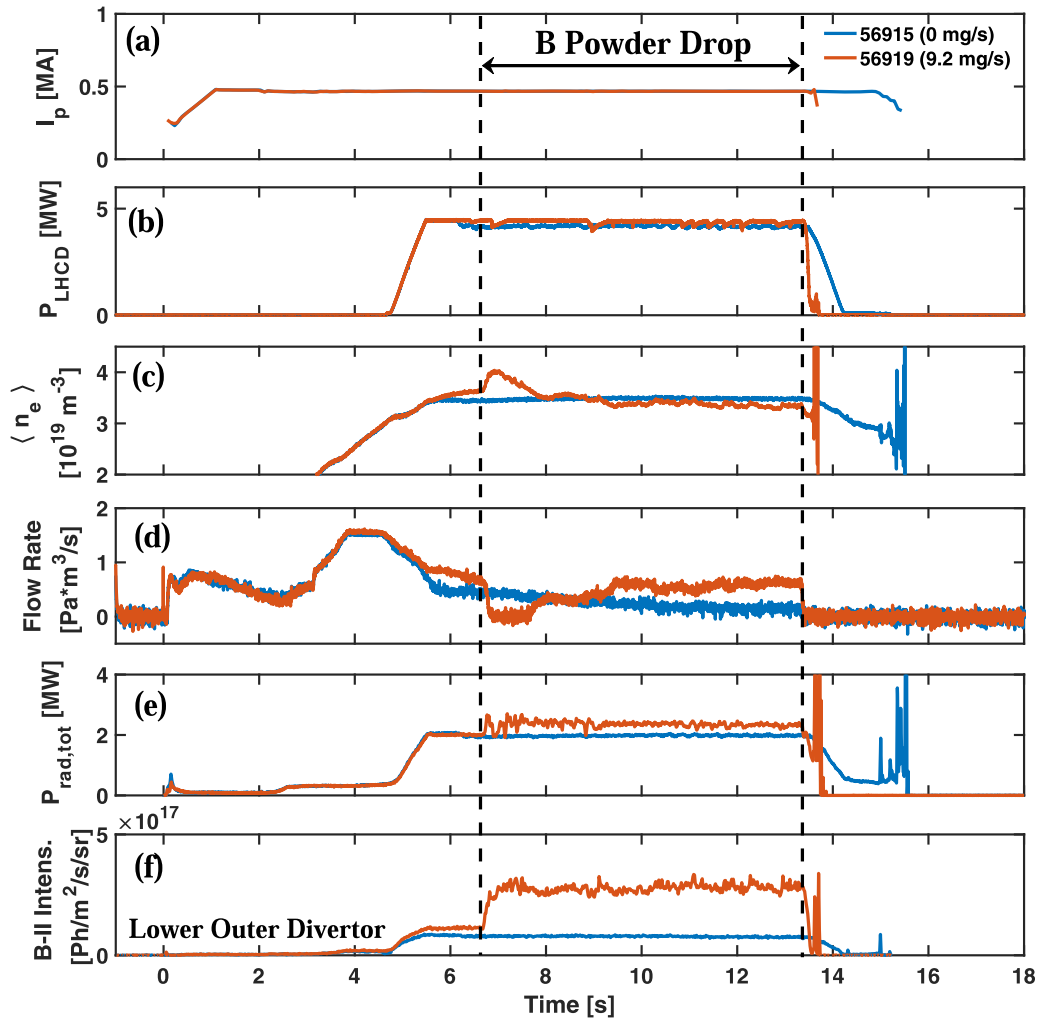


**Figure 2.** (a)  $I_p$ , (b)  $P_{LHCD}$ , (c)  $\langle n_e \rangle$ , (d)  $D_2$  fueling rate, (e)  $P_{rad,tot}$ , and (f) B-II line intensity at the lower outer divertor for a WEST discharge with (56919) and without (56915) B powder injection.

and then transported both toroidally around the top of the machine and to the high-field-side edge. This toroidal ablation plume has been observed in previous B powder injection experiments in LSN discharges on AUG [14].

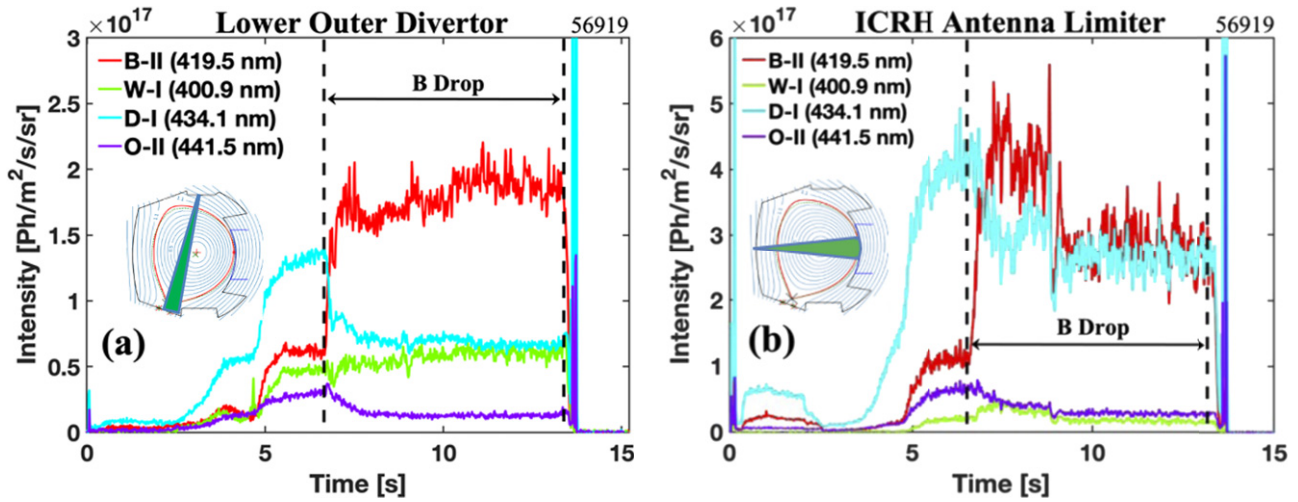
Over the course of several shots, the powder drop rate was varied to determine the optimal rate where the largest amount of powder could be dropped without invoking a disruption. This was found to be between  $9 \text{ mg s}^{-1}$  and  $17 \text{ mg s}^{-1}$ . Higher drop rates resulted in abrupt disruptions, most likely due to rapid increases in the electron density and radiated power. IPD experiments on other tokamaks and stellarators have sustained drop rates of  $>17 \text{ mg s}^{-1}$ , however these experiments typically utilized increased auxiliary power and/or different magnetic configurations [14, 16, 19, 21]. The number of B atoms injected per shot varied from  $2.7 \times 10^{20}$  to  $4.0 \times 10^{21}$  atoms depending upon the drop rate and drop duration. Cumulatively, 310 mg of B or  $1.74 \times 10^{22}$  B atoms were dropped over the 10 discharges.

Figure 2 shows the effect of B powder injection on several key plasma parameters. WEST discharges proved to be robust to powder injection as there were only minimal changes to the plasma current (figure 2(a)) and the LHCD power (figure 2(b))

during the entire B drop. The shot with B powder disrupts  $\sim 1 \text{ s}$  early due to an intervention from the infrared (IR) protection system unrelated to the B drop.

A small increase in the volume-averaged electron density (figure 2(c)) was observed when the powder was introduced to the plasma, however after 1 s, the density returned to the baseline level and ended up slightly lower than the discharge without powder injection. This reduction in density occurred concurrently with a programmed increase in the  $D_2$  flow rate (figure 2(d)), which was added to suppress IR interventions in the early phase of the discharge. Similar decreases in the electron density have been observed in B powder injection experiments on DIII-D [18].

There was a noticeable increase in the total radiated power, around 20% for a drop rate of  $9.2 \text{ mg s}^{-1}$ , that was sustained for the entire B drop. This increase was concentrated to the upper plasma edge, as central viewing chords did not observe any large increases in  $P_{rad}$  during the boron drop. The B-II (419.5 nm) line intensity at the lower outer divertor is shown in figure 2(e) to clearly demonstrate the duration of the B drop. The non-zero B-II signal in shot 56915 was due to the sputtering of intrinsic B from BN tiles installed on the centerstack



**Figure 3.** B-II (419.5 nm), W-I (400.9 nm), D $\gamma$  (434.1 nm), and O-II (441.5 nm) line intensities at (a) the lower outer divertor and (b) the ICRH antenna limiter. Viewing area shown in cartoon not to scale.

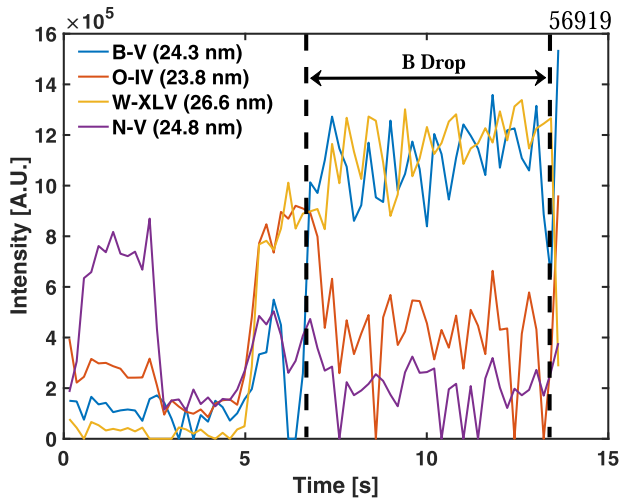


**Figure 4.** B-V (24.3 nm), O-IV (23.8 nm), W-XLV (26.6 nm), and N-V (24.8 nm) line intensities for Shot 56919 with  $9.2 \text{ mg s}^{-1}$  of B powder injection.

and the outer vessel walls for plasma startup. Previous GDB was unlikely to have impacted the B-II measurements given the number of discharges ( $>300$ ) between the last boronization and the IPD experiments. Overall, at modest drop rates, B powder injection was shown to be relatively non-perturbative to WEST L-mode discharges.

Due to diagnostic constraints, surface analysis of the PFCs could not be performed during or after the IPD experiments. Therefore, the number of B atoms deposited/eroded and the thickness of the deposited layers is still unknown. Surface analysis of probes inserted during B powder injection in DIII-D H-modes have estimated deposition rates to be  $\sim 1 \text{ nm s}^{-1}$  with coating efficiencies of  $0.1 \text{ nm mg}^{-1}$  of injected B [14]. The elemental composition of these surface layers was found to be 1:1 for B:C and 2.3 for B/O. Similar analyses will be done for WEST discharges in the upcoming C6 campaign. An insertable collector probe [23] will be used to measure the deposition of the injected B-10 atoms (used to

differentiate from the intrinsic B-11). In the absence of these results, spectroscopy and bolometry were used to obtain a general picture of the impact of boron powder injection on the full-W environment of WEST.

### 3. Real-time wall conditioning

#### 3.1. Wall conditioning during powder injection

Conditioning of the WEST PFCs was largely evaluated using an extensive visible spectroscopy (VS) system with views of several key PFCs [24]. This section will focus on VS measurements at the lower outer divertor, due to the LSN configuration, and at the ICRH antenna limiter, which was radially positioned 5 mm in front of the LHCD antennas and acted as the outboard limiting surface. The ICRH antenna, a potential source for gross W erosion [25], was placed here for comparison with powder-free W sourcing experiments that positioned the antenna in the same location [26]. No ICRH power was used during the powder injection experiments to keep consistency with the W sourcing experiments and to better isolate the effects of powder injection, as ICRH is known to significantly increase impurity sputtering in WEST [27].

The authors note that line radiation is dependent on the local  $T_e$  and  $n_e$ , and when possible, the species' particle flux should be used to make statements about wall conditioning. Due to diagnostic constraints, SOL  $T_e$  and  $n_e$  measurements were only available in the lower outer divertor region. Therefore, to compare the impact of powder injection at both the lower outer divertor and ICRH antenna limiter, only the calibrated visible line intensities were used. An estimation of the deuterium and impurity particle fluxes at the lower outer divertor is given in section 3.3.

The impact of B powder injection on the B-II (419.5 nm), W-I (400.9 nm), D $\gamma$  (434.1 nm), and O-II (441.5 nm) line intensities at the lower outer divertor and at the ICRH antenna limiter are shown in figure 3. The time traces correspond to the line-of-sight with the peak signal intensities from the array.



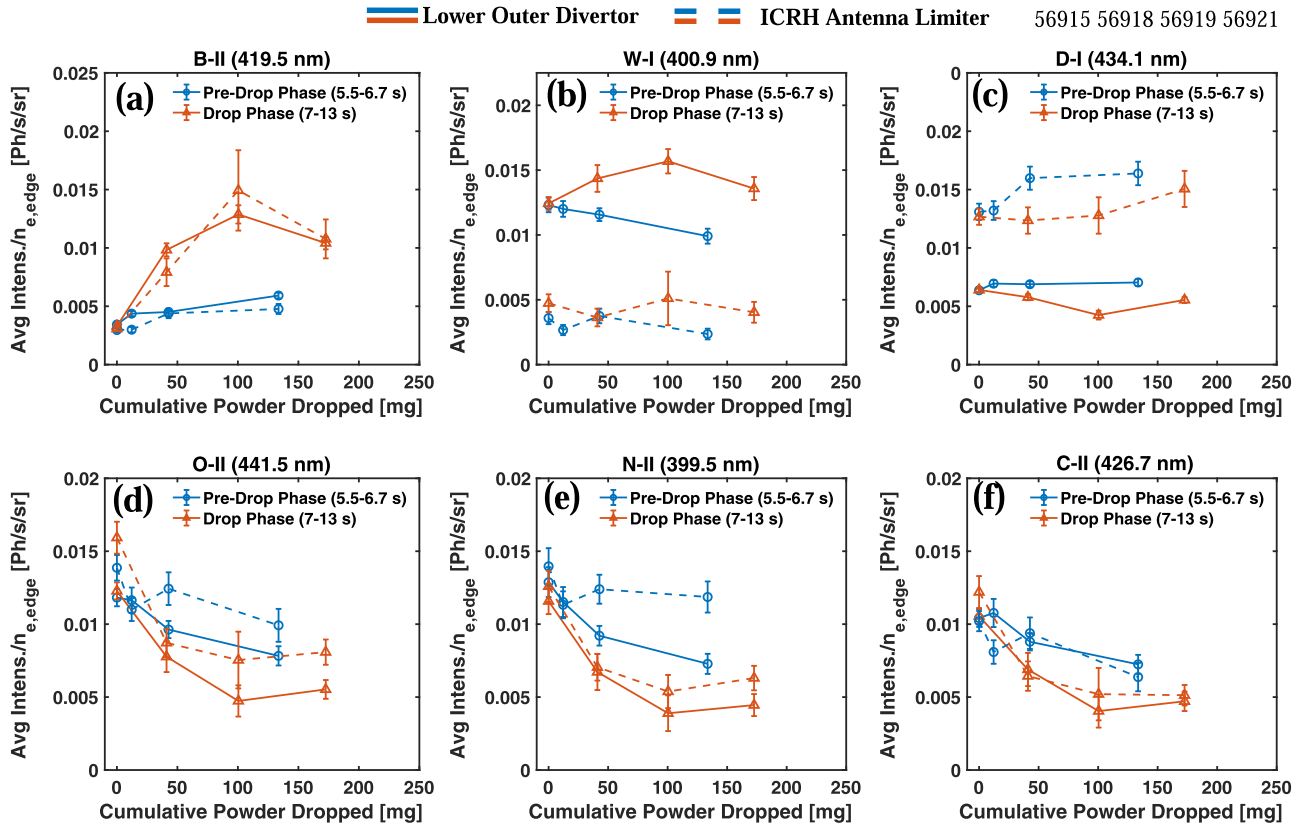


**Figure 5.** Density-normalized time-averaged line intensities for (a) B-II, (b) W-I, (c)  $D_\gamma$ , (d) O-II, (e) N-II, and (f) C-II at the lower outer divertor (solid lines) and the ICRH limiter (dashed lines). Blue circles correspond to the pre-drop phase (5.5–6.7 s) and the orange triangles correspond to the B powder drop (7–13 s).

These intensity traces were taken from shot 56919 (shown in figure 2) which had a B drop duration of 7 s with a drop rate of  $9.2 \text{ mg s}^{-1}$ . The B powder drop begins around 6.7 s, however all line intensities increased at 5 s due to the initiation of the LHCD heating/current drive system.

A rapid increase in the B-II signal was observed around 6.7 s at both viewing locations as soon as the powder was ablated by the plasma. This increase was coincident with decreases to the  $D_\gamma$  and O-II line intensities, suggesting a reduction in the deuterium recycling and/or oxygen sputtering. Similar trends were observed for N-II (399.5 nm) and C-II (426.7 nm), but these traces were not shown in figure 3 for clarity. The decrease in  $D_\gamma$ , C, O, and N line intensities are consistent with real-time wall conditioning of the W PFCs, even at the lower outer divertor which is located substantially downstream from the B drop location.

During powder injection, the W-I line intensity increased modestly. This increase occurred despite the fact that the oxygen, a known sputterer of tungsten, line intensity decreased. At both the lower outer divertor and the ICRH antenna limiter, the W-I signal followed the B-II signal, suggesting that B was the dominant W sputtering mechanism during powder injection. These results are consistent with observations from BN powder injection experiments in the full-W AUG tokamak [14].

A general idea of the radial penetration of W and other impurities can be deduced from vacuum ultraviolet (VUV)

spectroscopy. Ions inside the separatrix exist at higher charge states and radiate more intensely at lower wavelengths. Measurements from the WEST real-time VUV spectrometer (central chord view), shown in figure 4, additionally indicated increased B and W line intensities during the B drop and decreased O and N line intensities. The strong increase in the N-V line intensity from 0–3 s was due to the startup phase of the discharge which limits on the previously-mentioned BN tiles. Unfortunately,  $T_e$  measurements were only available in the SOL and not in the plasma edge due to pollution of the electron cyclotron emission (ECE) signal from LHCD. Therefore, it is difficult to make conclusions on the radial penetration of B and W from just the line intensities. While the B and W line intensities increased during the drop, core bolometry channels observed only minimal changes in the radiated power. Future experiments are needed to determine the particle fluxes of B and W crossing the separatrix.

### 3.2. Wall conditioning after powder injection

Following a discharge with B powder injection, the subsequent shots showed several indications of improved wall conditioning. To illustrate this, time-averages of the VS and VUV line intensities were calculated for the ‘pre-drop phase’ (i.e. the time between the LHCD turn-on and the start of the B drop) and the drop phase (i.e., the duration of the B powder drop). The pre-drop phase of the powder injection discharges was

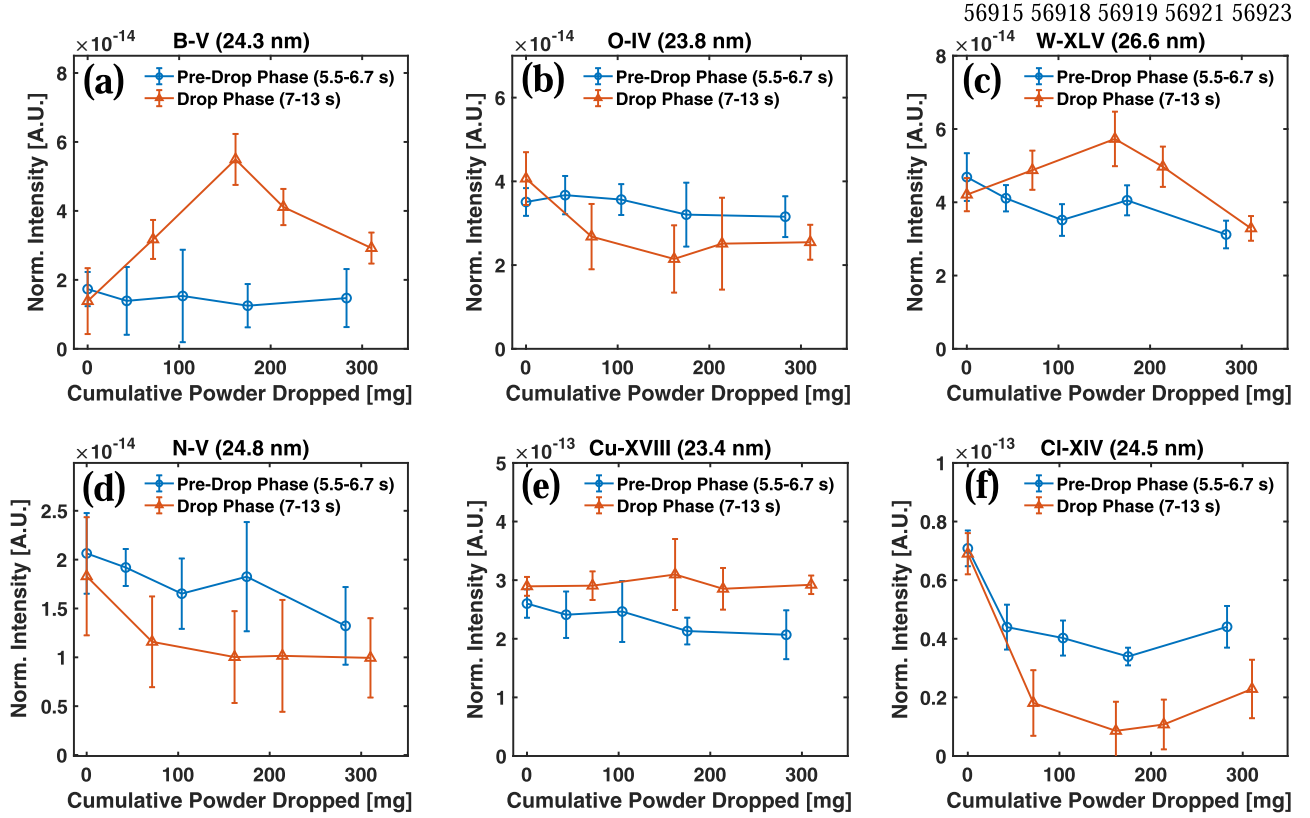


**Figure 6.** Density-normalized time-averaged line intensities for (a) B-V, (b) O-IV, (c) W-XLV, (d) N-V, (e) Cu-XVIII, and (f) Cl-XIV. Blue circles correspond to the pre-drop phase (5.5–6.7 s) and the orange triangles correspond to the B powder drop (7–13 s).

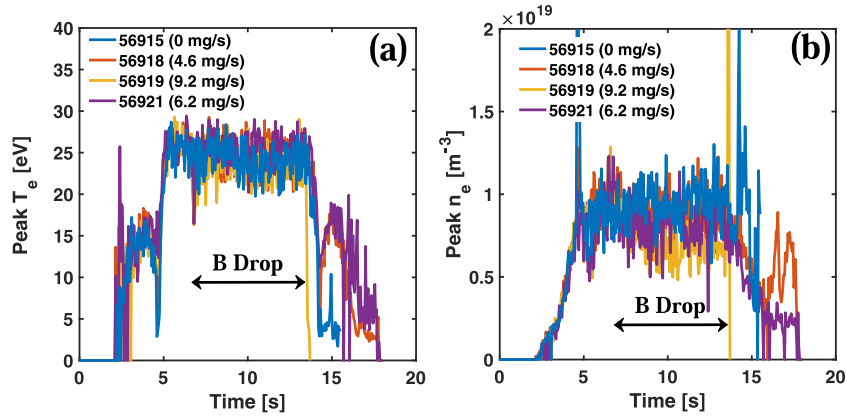


**Figure 7.** (a) Peak SOL  $T_e$  and (b) peak SOL  $n_e$  from the WEST divertor Langmuir probe array for a discharge without B injection and three discharges with B injection.

used to assess the conditioning effects of the preceding B powder drops. These time-averaged line intensities for multiple spectral lines in the visible range are shown in figure 5 as a function of the cumulative powder dropped in the preceding shots. The blue circles correspond to the pre-drop phase and the orange triangles correspond to the drop phase. The solid lines represent measurements taken at the lower outer divertor, while the dashed lines represent measurements taken at the ICRH antenna limiter. The blue circles and orange triangles are mismatched on the  $x$ -axis because the orange triangles consider that powder has been dropped not only in the preceding shots but during the discharge as well. Lastly, the traces

were normalized to the edge line-integrated density ( $\rho = 0.8$ , closest interferometry chord to the plasma edge) to account for any changes in electron density or fueling.

As more B powder was dropped, the pre-drop B-II line intensity (figure 5(a)) continually increased. This effect was observed at both the lower outer divertor and at the ICRH antenna limiter and may be an indication of thin-film deposition on the PFCs. Concurrently, decreases in the pre-drop W-I and O-II line intensities were observed. These trends agree qualitatively with similar traces from B powder injection experiments on the full-W AUG tokamak [14].

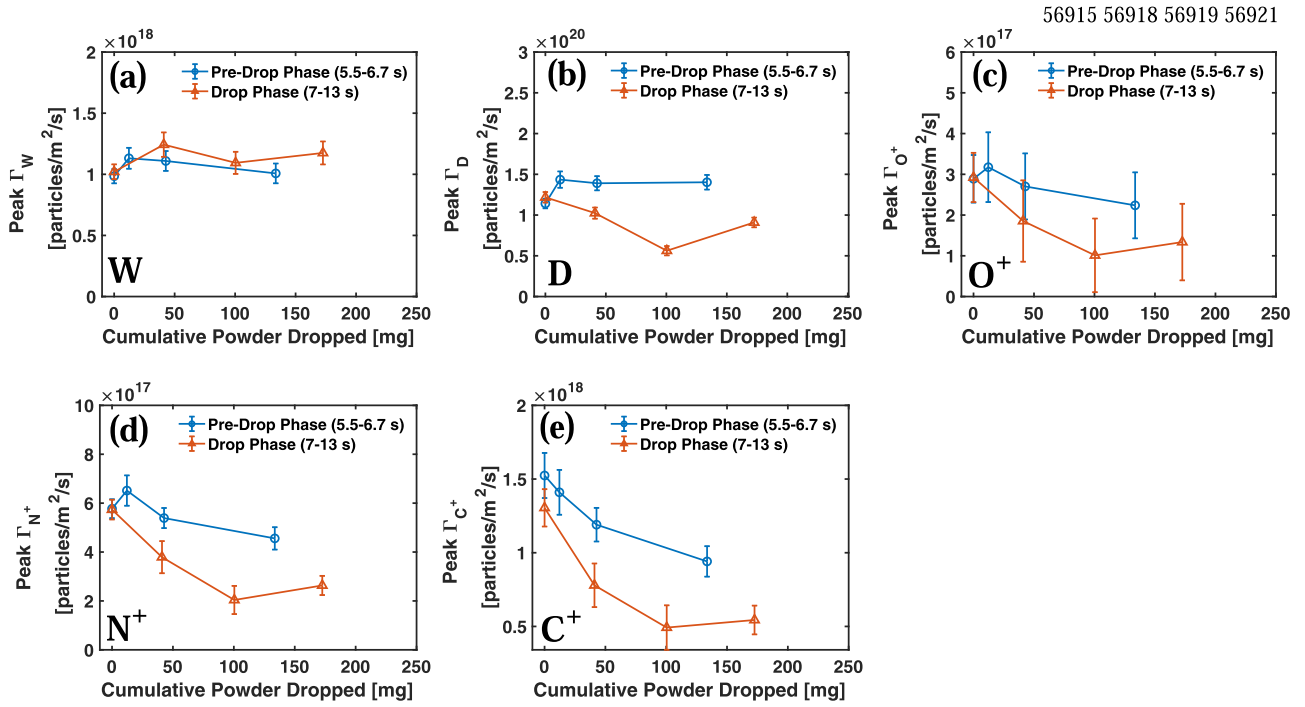


**Figure 8.** Peak particle fluxes for (a) W, (b) D, (c) O<sup>+</sup>, (d) N<sup>+</sup>, and (e) C<sup>+</sup> at the lower outer divertor. Blue circles correspond to the pre-drop phase (5.5–6.7 s) and the orange triangles correspond to the B powder drop (7–14 s).

While the decrease in W-I intensity is very encouraging, it was confined to the pre-drop period. During B injection (figure 5(b) orange triangles), the time-averaged W-I intensity always increased relative to the pre-drop level (figure 5(b) blue circles). The increase of the W-I line intensity from the pre-drop phase to the drop phase seemed to be stronger at the lower outer divertor than at the ICRH limiter, suggesting differing sputtering rates at those locations. This contrasts with BN powder injection experiments in AUG, which observed larger increases in the W-I signal at the midplane ICRH antenna limiter than at the lower outer divertor [14]. Some likely explanations for the difference in W sputtering observed in the two machines are differences in the confinement mode (L-Mode on WEST vs ELMy H-Mode on AUG), the electron density, the electron temperature, the distance between the separatrix and the ICRH antenna limiter, and the fueling and pumping configurations.

The B powder had a relatively benign effect on the pre-drop deuterium recycling at the lower outer divertor and resulted in an increase in recycling at the ICRH antenna limiter. This may be due to the release of D atoms trapped in the deposited B films from previous discharges. Nevertheless, the discharges following a B drop were all able to reliably maintain the target density, indicating that erosion of D from the B films was not an issue for density control.

Slightly different trends were observed in the VUV time-averaged line intensities. Figure 6 shows edge density-normalized time-averages for B-V (24.3 nm), O-IV (23.8 nm), W-XLV (26.7 nm), N-V (24.8 nm), Cu-XVIII (23.4 nm), and Cl-XIV (23.8 nm) before and during the B drop. In contrast to the VS measurements, the pre-drop B signal (blue circles in figure 6(a)) stays relatively constant as more power was

dropped. This may imply that even though a B film has been deposited onto the PFCs, there is not a significant flux of B through the separatrix. Similar to VS, decreases in the pre-drop W, O, and N line intensities were observed. Powder injection resulted in a decrease in the pre-drop copper and chlorine line intensities as well. These results were obtained by only injecting  $\sim 310$  mg of B powder (GDB can use up to 40 g of diborane gas [28]), which motivates the injection of larger quantities of powder in the future.

### 3.3. Estimation of impurity particle fluxes

While trends in the spectroscopic line intensities can provide valuable information, the line emission is influenced by the local  $T_e$  and  $n_e$ . Therefore, the species' particle flux is a better representation of the impact of B powder injection. Particle flux for a given ion species can be determined by multiplying the calibrated line intensity from spectroscopy with its corresponding S/XB (ionizations per photon) coefficient. These coefficients are dependent upon the local electron temperature and electron density, and hence consider the effect of the background plasma. This method and the definition of the S/XB coefficients are detailed extensively in [29].

Visible spectroscopy data at the lower outer divertor were S/XB corrected using measurements from an array of flush-mounted Langmuir probes embedded in the divertor target [30]. The SOL measurements and resultant particle flux estimates are therefore highly localized to that location. The peak values of  $T_e$  and  $n_e$  from the Langmuir probe array are shown in figures 7(a) and (b) for the discharges in figure 5. Similar to the volume-average density in figure 2(c), the SOL  $n_e$  increased at the start of powder injection but was then reduced below the



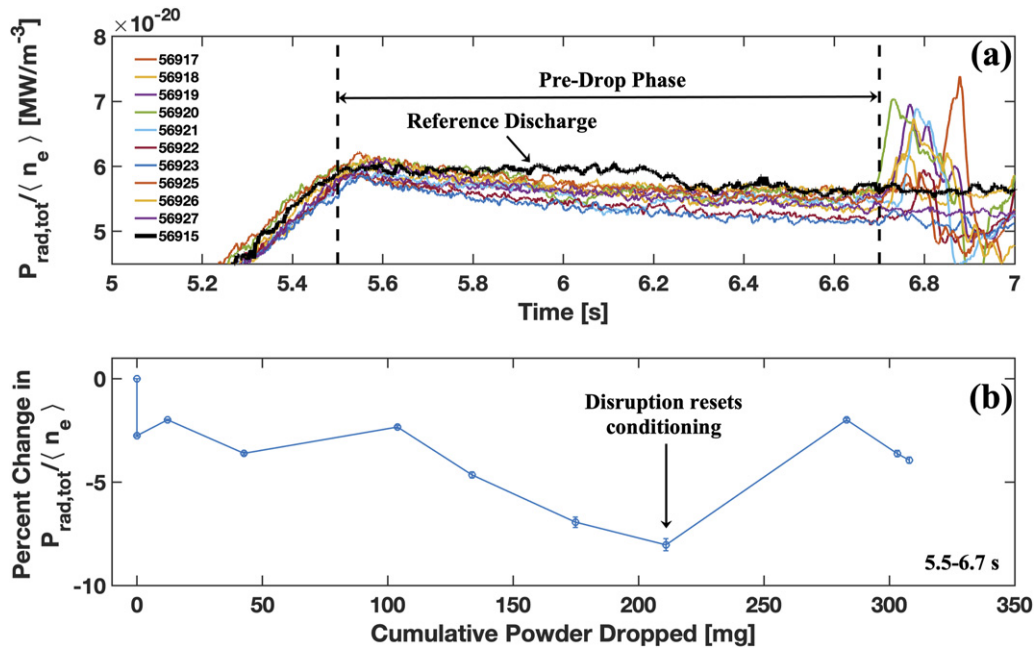


**Figure 9.** (a) Density-normalized total radiated power (all traces have varying levels of B powder injection except for 56915). (b) Percent change in the time-averaged  $P_{\text{rad,tot}} / \langle n_e \rangle$  for the discharges in figure 9(a) during the pre-drop phase.

reference level (blue trace) as powder injection continued. In fact, this trend was more pronounced at the SOL, as  $9.2 \text{ mg s}^{-1}$  of B powder injection (yellow trace) resulted in almost a 40% reduction of the electron density. The reduction in  $n_e$  additionally seemed to correlate with the powder drop rate and this is explored further in section 4.2. Lastly, the electron temperature changed minimally, possibly due to competing effects from the introduction of radiating impurities and the reduction in  $n_e$ .

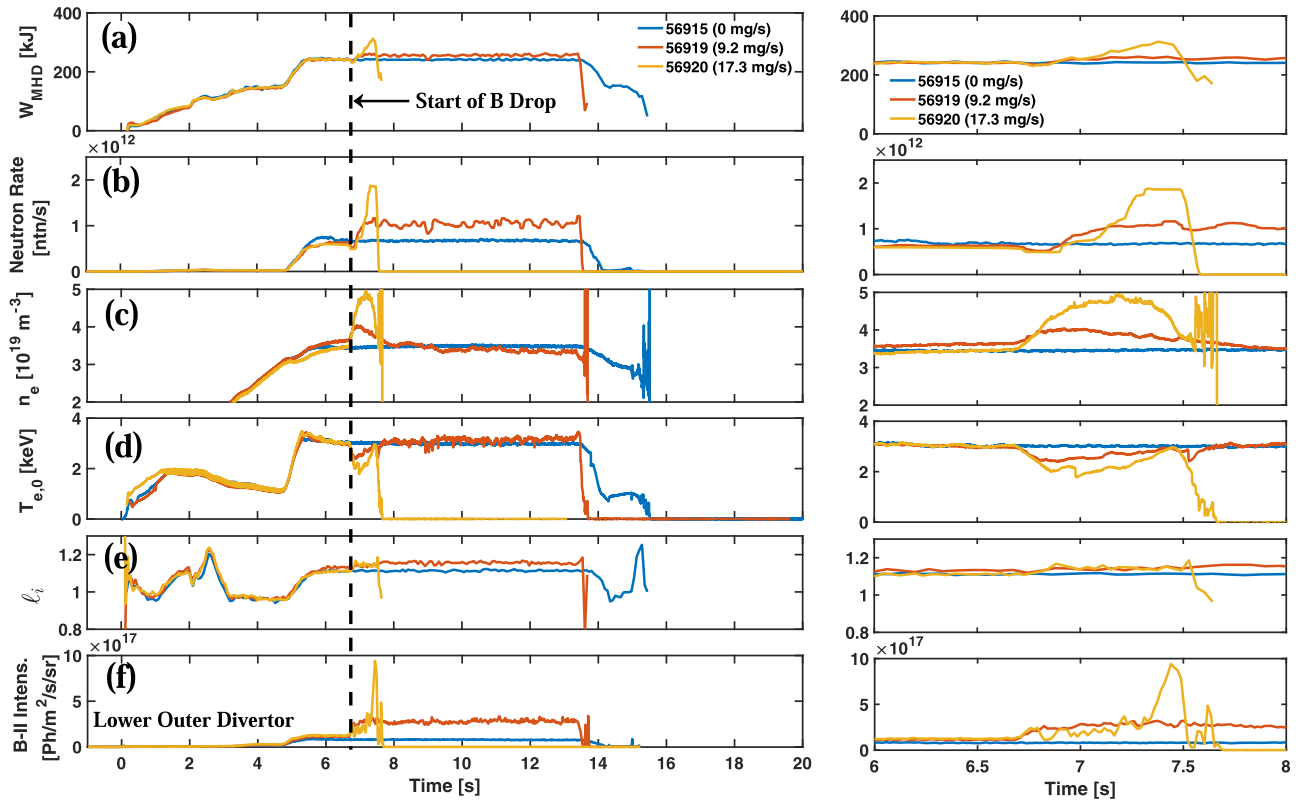
Particle fluxes for species with available S/XB coefficients (W, D,  $\text{O}^+$ ,  $\text{N}^+$ , and  $\text{C}^+$ ) were calculated for several B powder discharges at the lower outer divertor. S/XB coefficients were obtained using ColRadPy [31], a python module that solves the collisional radiative equations for a better approximation of the S/XBs. The peak particle flux at the lower outer divertor for several ion species are shown in figure 8 as a function of the cumulative powder dropped similar to figure 5. Once again, the blue circles correspond to the pre-drop phase and the orange triangles correspond to the drop phase.

Figure 8(a) confirms that the increase in W-I line intensity during the powder drop (figure 3(a)) corresponds to an increase in the W particle flux ( $\sim 20\%$  in the largest instances). The initial increase in the pre-drop W,  $\text{O}^+$ , and  $\text{N}^+$  particle fluxes (second blue circle in figures 8(a), (c) and (d)) may be due to a programmed increase in the electron density target, as no B powder was dropped in the reference discharge. While the S/XBs should account for this increase in electron density, the increased gas fueling may have additionally contributed to an increase in the neutral D density. This is evidenced by the increased pre-drop D flux in figure 8(b), which may then have resulted in further impurity sputtering.

Despite this, the pre-drop W particle flux continually decreased in the subsequent shots following B powder injection (10% reduction between the second and fourth blue circles in figure 8(a)). The impact of B powder injection on low-Z impurity particle fluxes was even more pronounced as reductions in the pre-drop particle fluxes were up to 50% (blue circles in figures 8(c)–(e)) and reductions in the particle flux during the B drop ranged from 40%–60% (difference between blue circles and orange triangles in figures 8(c)–(e)). Similar to the VS measurements, discharges with B powder showed large reductions in recycling during the B drop, but no large changes to the recycling in the subsequent discharges. These results confirm that the reduction in line intensities observed by VS was likely to be consistent with conditioning of the PFCs. Future experiments will characterize the change in particle flux at the ICRH antenna limiter and other possible locations of gross W erosion.

#### 3.4. Impact of powder injection on the total radiated power

Along with the spectroscopy and particle flux results, B powder injection had a significant impact on the total radiated power. Figure 9(a) shows the total radiated power measured by the WEST bolometer array, normalized to the volume-averaged electron density, for all B powder injection discharges and for a reference discharge without B power injection (56915—thick black trace). While B powder injection substantially increased  $P_{\text{rad,tot}}$  during injection, the subsequent discharges generally had lower levels of  $P_{\text{rad,tot}}$  in the pre-drop phase. To better visualize this, the signals in figure 9(a) were averaged from 5.5–6.7 s and then compared to the initial reference value. A clear reduction in the total  $P_{\text{rad,tot}} / \langle n_e \rangle$



**Figure 10.** (a)  $W_{\text{MHD}}$ , (b) neutron rate, (c) volume-averaged  $n_e$ , (d) central electron temperature  $T_{e,0}$ , (e) internal inductance  $\ell_i$ , and (f) B-II line intensity at the lower outer divertor for WEST discharges with varying B powder drop rates. The panels on the right show a closer look at the time window from 6–8 s.

was observed as more powder was dropped in the preceding discharges.

The substantial increase in radiated power after 200 mg was attributed to a ‘large’ disruption at the end of the 8th powder injection discharge (shot 56 923). Not all disruptions led to a degradation in wall conditioning (i.e., increased  $P_{\text{rad,tot}}/\langle n_e \rangle$ ). In the case of shot 56 923, the disruption is considered large as the subsequent shot (56 924) was unable to breakdown, and the shot after that (56 925) disrupted early, presumably due to the large outgassing from the initial disruption event. After powder injection was resumed in shot 56 926, the total radiated power began to decrease again.

Due to the small amount of powder injected in these experiments, the deposited films were likely much thinner than those from standard GDB. Film thickness is typically taken as a figure of merit for conditioning and stability of the deposited layers [8]. Therefore, avoiding disruptions is critical until thicker coatings of B are developed. Nevertheless, the reduction in  $P_{\text{rad,tot}}/\langle n_e \rangle$  motivates further use of the IPD as a mechanism to extend the operational domain of WEST to higher densities.

Future experiments are needed to determine if the IPD can facilitate H-mode access on WEST. Reducing the influx of C, O, N, and W will conceptually increase the amount of power that crosses the separatrix by limiting radiative losses. Unfortunately, due to operational constraints, these initial powder injection experiments only had  $P_{\text{aux}} = 4.5$  MW available with  $P_{\text{rad,tot}} \sim 2\text{--}2.5$  MW. Therefore, the resultant input power

( $\sim 2$  MW) was under the predicted WEST L-H power threshold from both the 2004 and 2008 ITPA scalings [6]. The next run campaign will feature discharges with increased auxiliary power for a better evaluation of the impact of powder injection on H-mode access in WEST.

## 4. Improvements in confinement

### 4.1. Experimental observations of improved confinement

In addition to the improved wall conditions, WEST discharges with B powder injection had improved energy confinement. The impact of B powder injection on the plasma stored energy, the neutron rate (used here as a proxy for the central ion temperature), volume-averaged electron density, central electron temperature, and the internal plasma inductance is shown in figure 10. The three discharges in figure 10 correspond to a discharge without B powder injection (56 915), a discharge with a moderate B powder drop rate (56 919), and a discharge with a high B powder drop rate (56 920). The short drop period of 56 920 was due to an early disruption from the rapid drop rate. While 56 920 observed the largest improvement in confinement, it is difficult to make conclusions based on this discharge due to its short duration.

Both discharges with B powder injection had increased stored energy and an increased neutron rate for the entire drop duration; hence, this is believed not to be a transient effect. These increases in stored energy and neutron rate were

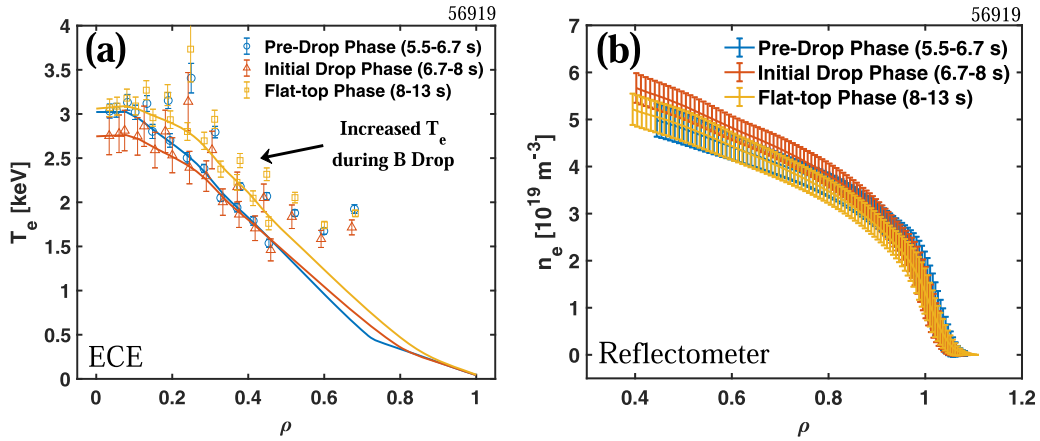


**Figure 11.** (a) Time-averaged ECE measurements of  $T_e(\rho)$  and their corresponding fits. (b) Time-averaged reflectometry measurements of  $n_e(\rho)$ . Colors/symbols denote the time-average windows used: pre-drop phase (blue/circles), initial drop phase (red/triangles), and flat-top phase (yellow/squares).

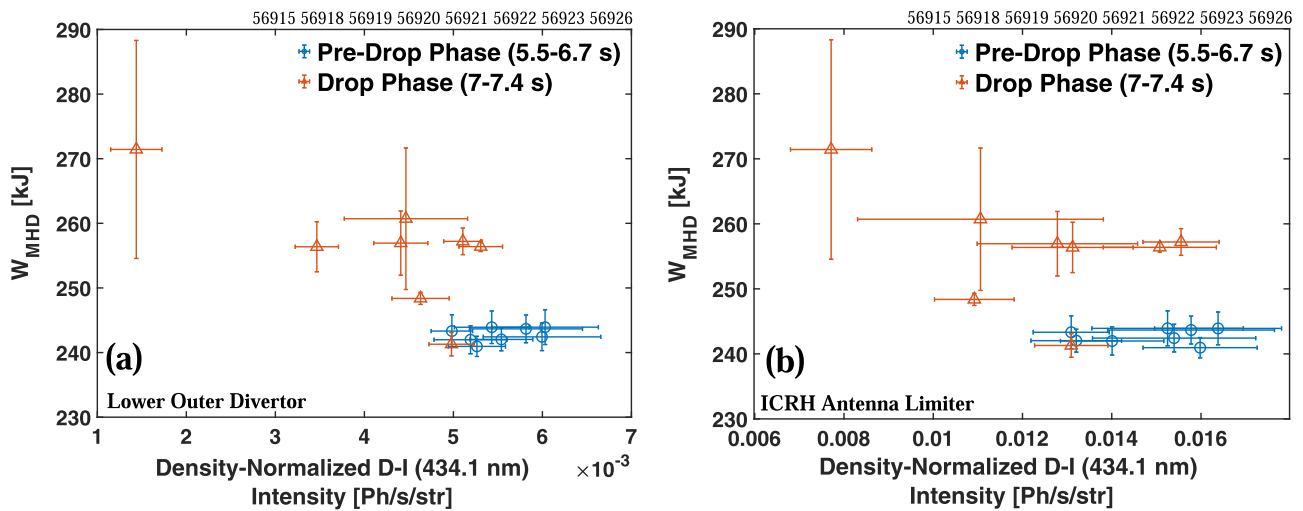


**Figure 12.** Time-averaged  $W_{\text{MHD}}$  vs edge normalized  $D_\gamma$  line intensity at the lower outer divertor (a) and the ICRH antenna limiter (b). The orange triangles correspond to the pre-drop phase and the blue circles correspond to the drop phase.

concurrent with increases in radiated power and electron density (shown for 56919 in figures 2(e) and 10(c)), suggesting improved confinement to maintain the same level of  $I_p$  without increasing  $P_{\text{LHCD}}$  or  $P_{\text{OH}}$ . Similar improvements in confinement have been observed in previous boron-based powder injection experiments in AUG [14, 15], LHD [21, 22], and W7-X [20].

In addition to the improvements in stored energy and neutron rate, the central electron temperature increased after the initial drop period (figure 10(d)). Further analysis shows that this increase in temperature was complemented by a broadening of the  $T_e$  profile up to  $\rho = 0.5$ . This can be seen in figure 11(a) which shows ECE measurements of  $T_e(\rho)$  and their corresponding fits. The profiles were taken from shot 56919 ( $9.2 \text{ mg s}^{-1}$  of B powder injection) and were averaged over the pre-drop phase (5.5–6.7 s), initial B drop phase (6.7–8 s), and the density flat-top phase (8–13 s). There is a large disparity between the ECE measurements and the fitted profile at  $\rho > 0.5$  due to signal pollution from the LHCD antennas.

These ECE measurements are accompanied by reflectometry profiles (figure 11(b)) averaged over the same time-windows to provide an indication of the density profile structure. During the initial drop phase (red profiles/triangles), the core density increased above the pre-drop level (blue profiles/circles) and the electron temperature decreased in response, keeping the electron pressure approximately constant. After this initial phase of the B drop, the majority of the density profile (yellow) was reduced, however the core density still remained slightly higher than the pre-drop level. This coupled with an increase in the electron temperature resulted in a higher electron pressure than during the pre-drop phase.

While both the neutron rate and  $W_{\text{MHD}}$  increased almost immediately with the onset of powder injection, the electron temperature only increased after the electron density returned to the pre-drop level. The increase in temperature was most pronounced from  $\rho \sim 0.2$ – $0.5$ , resulting in a significant broadening of the  $T_e$  profile. Unlike the increases in stored

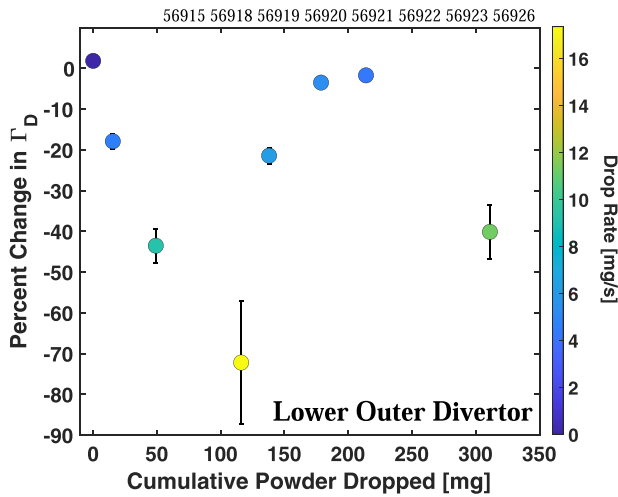


**Figure 13.** Percent change in  $\Gamma_D$  from the pre-drop phase (5.5–6.7 s) to the drop phase (7–7.4 s) vs the cumulative powder dropped in previous discharges at the lower outer divertor. The color of the data points corresponds to the drop rate.

energy and neutron rate, this phenomenon was confined to discharges with sustained durations of powder injection ( $t_{\text{drop}} > 1$  s). In discharges with pulsed injection ( $t_{\text{drop}} \sim 400$  ms), the same decrease in  $T_e$  was observed during the initial B drop phase, however the  $T_e$  profile never reached the elevated state observed in discharges with  $t_{\text{drop}} > 1$  s.

The improvements in confinement may be similar to those from gaseous impurity seeding experiments. Improved plasma performance due to the injection of impurities has been previously observed on a number of tokamaks [32–34], most notably with the radiative-improved (RI) mode [35] on TEXTOR. The increase in confinement is first triggered by fuel dilution (i.e., increased  $Z_{\text{eff}}$ ) which then leads to a bifurcation in the density profile once a critical value of  $Z_{\text{eff}}$  is obtained [35]. After a peaked density profile is established, it becomes the dominant mechanism for suppression of ion temperature gradient-driven turbulence. B<sub>4</sub>C powder injection experiments in W7-X have observed results reminiscent of the RI-mode with peaked core density profiles and increased  $Z_{\text{eff}}$  leading to improved plasma performance [20].

On the other hand, gaseous N<sub>2</sub> seeding experiments on WEST [36] have observed increases in confinement without density profile modification. In these experiments, fuel dilution was the dominant mechanism for turbulence suppression. Unfortunately, uncertainties in the visible bremsstrahlung signal prevented measurements of  $Z_{\text{eff}}$  during powder injection. Resistive estimates of  $Z_{\text{eff}}$ , calculated during the Ohmic phase of the discharge (0–5 s), showed no large changes following a discharge with B powder injection. Therefore, further analysis and experiments are needed to understand the impact of powder injection on core confinement. To confirm the dominant turbulence suppression mechanism(s), future powder injection experiments will utilize multiple species of B powder (B and BN) to isolate the role of  $Z_{\text{eff}}$  and increased quantities of powder to reach the critical  $Z_{\text{eff}}$  for density profile bifurcation. These experiments will be complemented by

interpretative modelling using METIS [37] and gyrokinetic simulations using QuaLiKiz [38].

#### 4.2. Empirical correlations of improved confinement

Without a confirmed hypothesis behind the improvements in confinement, we rely on correlations from empirical observations to exploit this effect in future experiments. Further investigation suggests a correlation between the stored energy and the level of recycling at the lower outer divertor. Figure 12 shows the time-averaged stored energy plotted against the time-averaged  $D_\gamma$  intensity (taken as a proxy for recycling) at the lower outer divertor (a) and the ICRH antenna limiter (b). The  $D_\gamma$  line intensities have been normalized by the edge  $n_e$  (same interferometry chord used in figure 5) to account for any changes in external fueling. The blue circles correspond to time-averages of the pre-drop phase, while the orange triangles correspond to time-averages during the initial B powder drop. The stored energy signals during the B drop were only evaluated from 7–7.4 s to include discharges with high drop rates that disrupted shortly ( $< 2$  s) after the start of the drop. A clear linear trend between the stored energy and the recycling at both the divertor and the ICRH antenna limiter was observed as the discharges with the largest stored energy additionally had the lowest  $D_\gamma$  line intensity. This may be supported by the fuel dilution hypothesis, as decreasing the wall recycling reduces a potential deuterium fueling source, further increasing the  $Z_{\text{eff}}$  and possibly leading to a larger improvement in confinement.

Understanding the mechanisms behind the reductions in recycling are critical to exploiting these observed improvements in confinement. The two independent variables during the B powder injection experiments were the powder drop rate and the amount of powder dropped in the preceding shots. Figure 13 shows the effect of each of these parameters on the deuterium particle flux, only shown at the divertor due to the availability of local  $T_e$  and  $n_e$  measurements. The y-axis corresponds to the percent change in D particle flux from the pre-drop phase (5.5–6.7 s) to the drop-phase (7–7.4 s). The B powder drop rate appeared to be the primary influence on the reduction in recycling at the lower divertor. High powder drops rates led to the lowest reductions in recycling, while discharges with low drop rates and  $> 100$  mg of B dropped in the preceding shots observed minimal reductions in recycling. This is consistent with the results in figures 5(c) and 8(b) where the  $D_\gamma$  line intensity/particle flux was impacted during the actual B drop but the pre-drop  $D_\gamma$  line intensity/particle flux remained relatively unchanged in the subsequent discharges.

Looking at other quantities with respect to drop rate, it is clear that higher drop rates lead to larger improvements in confinement. Figure 14(a) shows that both the stored energy and neutron rate increased strongly and possibly non-linearly with increasing drop rate. Here, the data represents time-averages from discharges with sustained periods of improved confinement ( $> 4$  s). Figure 14(b) shows a similar but smaller effect on the electron temperature at different values of normalized radius. While the central electron temperature changed minimally with drop rate, the profile became increasingly broad



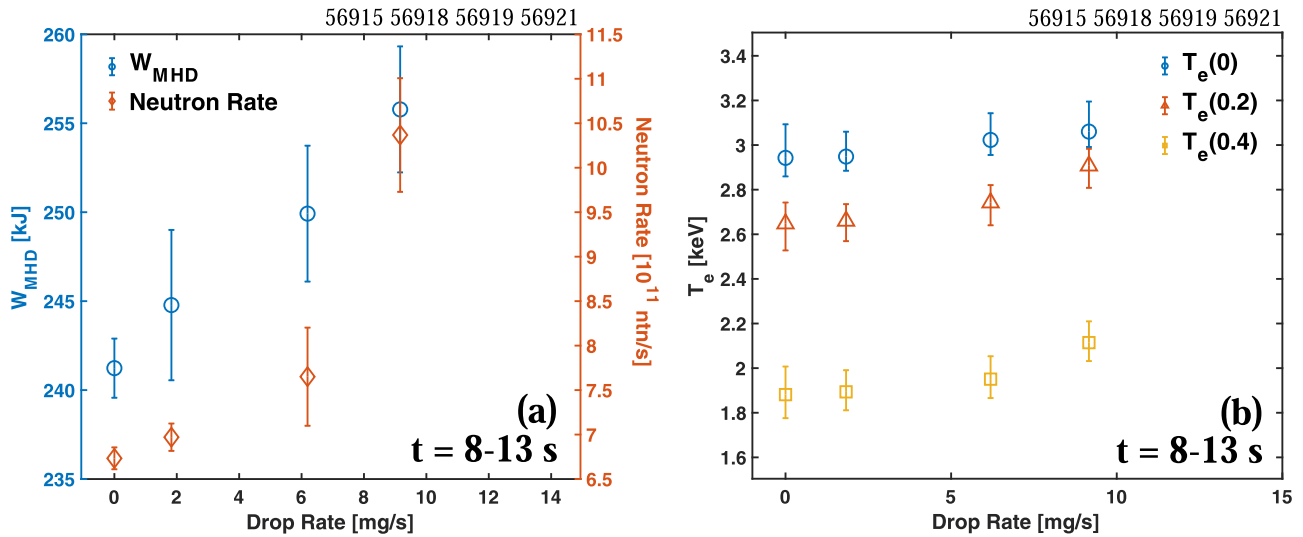


**Figure 14.** (a) Time-averaged  $W_{\text{MHD}}$  (blue circles) and neutron rate (orange triangles) vs powder drop rate in discharges with sustained increases in confinement. (b) Time-averaged  $T_e$  at  $\rho = 0$  (blue circles),  $\rho = 0.2$  (orange triangles) and  $\rho = 0.4$  (yellow squares) as a function of powder drop rate.

as the powder drop rate was increased. Mapping the improved performance parameter space will be critical to exploiting this phenomenon in the future. Especially since the main ion concentration can only be diluted so much before the increased radiation affects stability and/or the plasma becomes undesirable for fusion yields.

These results motivate the use of higher drop rates in future experiments due to the potential for even greater improvements in confinement and the ability to drop more powder for a given duration. Unfortunately, discharges with high B powder drop rates have proven to be more prone to disruption due to the rapid increase in electron density and radiated power. Increasing the auxiliary power should enable the sustainment of higher powder drop rates. A similar trend was observed in ELM suppression experiments on EAST as the drop rate required for ELM suppression increased with the heating power [39]. Future powder injection experiments on WEST will likely require  $P_{\text{aux}} > 5$  MW to sustain powder drop rates of  $> 17$  mg  $\text{s}^{-1}$ .

## 5. Conclusion

An IPD was successfully installed and commissioned on WEST. B powder was dropped into 10 LSN L-mode discharges with  $P_{\text{LHCD}} \sim 4.5$  MW and improvements in both wall conditions and plasma confinement were observed.

During the B powder drop, visible and VUV spectroscopy measurements showed reductions in deuterium recycling, low-Z impurity signals, and an increase in the W signal at both the ICRH antenna limiter and the lower outer divertor. As more powder was dropped, clear reductions in the pre-drop level of W-I and O-II were observed, indicating a cumulative conditioning effect from the powder and possible B thin film deposition. Estimates of the impurity particle flux using S/XB coefficients from ColRadPy [31] confirm these trends. Similar results were observed in the radiative power, as the

pre-drop  $P_{\text{rad,tot}}/\langle n_e \rangle$  continued to decrease as more powder was dropped. These conditioning effects appeared to reset after large disruptions which may have ablated the previously deposited B coatings. Nevertheless, these initial results are encouraging and prompt further investigation of B powder injection as a real-time wall conditioning technique for superconducting fusion devices.

In addition to the improved wall conditioning, sustained improvements in the stored energy (up to 11%), the neutron rate (up to 60%), and the electron temperature (up to 50% from  $\rho \sim 0.2-0.5$ ) were observed in discharges with B powder injection. Larger increases in the stored energy (up to 25%) and the neutron rate (up to 200%) were additionally observed, however, on much smaller time scales and preceding a disruption. These improvements occurred with no changes to the LHCD power or plasma current and were concurrent with increases in the electron density and radiated power, suggesting improved confinement. A likely explanation is the suppression of ITG-driven turbulence due to main ion dilution, as observed in  $\text{N}_2$  seeding experiments in WEST [36], and/or modification of the density profile, as observed in powder injection experiments on AUG [15], W7-X [20], and LHD [22].

These improvements in confinement appeared to correlate with a reduction in the D recycling, possibly due to further fuel dilution. This effect was observed at both the lower outer divertor and at the ICRH antenna limiter. The powder drop rate was determined to be the dominant actuator for reducing the D recycling, as discharges with the highest drop rates had the largest reductions in D line intensity/particle flux and the largest improvements in confinement.

The results presented in this paper have provided an initial basis from which to exploit future IPD operation on WEST. The upcoming C6 campaign will be the first with an all ITER-like PFU lower divertor and will evaluate long-pulse H-mode discharges in a full W environment. The experiments during the C5 campaign observed significant improvements in both



wall conditioning and plasma confinement using only 310 mg of B powder. Planned IPD experiments for the next campaign will extend these conditioning results by dropping powder for longer durations, utilizing higher drop rates, and comparing the impact of dropping BN powder with B powder.

## Acknowledgments

The authors would like to thank the WEST team and the ORNL PMI group for their support of the IPD experiments (particularly J. Morales, M. De Combarieu, J.F. Artaud, D. Vizinet, C. Gil, A. Grosjean, and C. Johnson), and gratefully acknowledge R. Maingi for useful discussion. This manuscript is based upon work supported by the US Department of Energy, Office of Science, Office of Fusion Energy Sciences, and has been authored by Princeton University under Contract Number DE-AC02-09CH11466 with the US Department of Energy. The publisher, by accepting the article for publication acknowledges, that the United States Government retains a non-exclusive, paid-up, irrevocable, world-wide license to publish or reproduce the published form of this manuscript, or allow others to do so, for United States Government purposes.











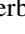
## Data availability statement

The datasets generated during and/or analyzed during the current study are available at <http://arks.princeton.edu/ark:/88435/dsp01cr56n4150>.

## Conflict of interest

The authors have no conflicts to disclose.

## ORCID iDs

G. Bodner  <https://orcid.org/0000-0003-2497-9172>  
 A. Gallo  <https://orcid.org/0000-0002-7472-7830>  
 A. Diallo  <https://orcid.org/0000-0002-0706-060X>  
 R. Lunsford  <https://orcid.org/0000-0003-3588-6801>  
 Ph. Moreau  <https://orcid.org/0000-0002-2868-7401>  
 C. Bourdelle  <https://orcid.org/0000-0002-4096-8978>  
 P. Manas  <https://orcid.org/0000-0002-0414-746X>  
 A. Bortolon  <https://orcid.org/0000-0002-0094-0209>  
 C.C. Klepper  <https://orcid.org/0000-0001-9107-8337>  
 E.A. Unterberg  <https://orcid.org/0000-0003-1353-8865>  
 L. Vermare  <https://orcid.org/0000-0002-3090-2713>

## References

- [1] Winter J. 1996 Wall conditioning in fusion devices and its influence on plasma performance *Plasma Phys. Control. Fusion* **38** 1503–42
- [2] Joffrin E. et al 2014 First scenario development with the JET new ITER-like wall *Nucl. Fusion* **54** 013011
- [3] Beurskens M.N.A. et al 2013 The effect of a metal wall on confinement in JET and ASDEX Upgrade *Plasma Phys. Control. Fusion* **55** 124043
- [4] Lipschultz B. et al 2007 Operation of alcator C-mod with high-Z plasma facing components and implications *Phys. Plasmas* **13** 056117
- [5] Bucalossi J. et al 2014 The WEST project: testing ITER divertor high heat flux component technology in a steady state tokamak environment *Fusion Eng. Des.* **89** 907–12
- [6] Bourdelle C. et al 2015 WEST physics basis *Nucl. Fusion* **55** 063017
- [7] Pitts R.A. et al 2013 A full tungsten divertor for ITER: physics issues and design status *J. Nucl. Mater.* **438** S48–56
- [8] Buzhinskij O.I. and Semenets Y.M. 1997 Review of *in situ* boronization in contemporary tokamaks *Fusion Technol.* **32** 1–13
- [9] Bucalossi J. et al 2022 Operating a full tungsten actively cooled tokamak: overview of WEST first phase of operation *Nucl. Fusion* **62** 042007
- [10] Zuo G.Z., Hu J.S., Zhen S., Li J.G., Mansfield D.K., Cao B., Wu J.H. and Zakharov L.E. (the EAST Team) 2011 Comparison of various wall conditionings on the reduction of H content and particle recycling in EAST *Plasma Phys. Control. Fusion* **54** 015014
- [11] Kallenbach A. et al 2009 Non-boronized compared with boronized operation of ASDEX Upgrade with full-tungsten plasma facing components *Nucl. Fusion* **49** 045007
- [12] Nagy A. et al 2018 A multi-species powder dropper for magnetic fusion applications *Rev. Sci. Instrum.* **89** 10K121
- [13] Kallenbach A. et al 2013 Impurity seeding for tokamak power exhaust: from present devices via ITER to DEMO *Plasma Phys. Control. Fusion* **55** 124041
- [14] Bortolon A. et al 2019 Real-time wall conditioning by controlled injection of boron and boron nitride powder in full tungsten wall ASDEX Upgrade *Nucl. Mater. Energy* **19** 384–9
- [15] Lunsford R. et al 2019 Active conditioning of ASDEX Upgrade tungsten plasma-facing components and discharge enhancement through boron and boron nitride particulate injection *Nucl. Fusion* **59** 126034
- [16] Sun Z. et al 2021 Suppression of edge localized modes with real-time boron injection using the tungsten divertor in EAST *Nucl. Fusion* **61** 014002
- [17] Xu W. et al 2021 Comparison of active impurity control between lithium and boron powder real-time injection in EAST *Phys. Scr.* **96** 124034
- [18] Bortolon A. et al 2020 Observations of wall conditioning by means of boron powder injection in DIII-D H-mode plasmas *Nucl. Fusion* **60** 126010
- [19] Gilson E.P. et al 2021 Wall conditioning and ELM mitigation with boron nitride powder injection in KSTAR *Nucl. Mater. Energy* **28** 101043
- [20] Lunsford R. et al 2021 Characterization of injection and confinement improvement through impurity induced profile modifications on the Wendelstein 7-X stellarator *Phys. Plasmas* **28** 082506
- [21] Nespoli F. et al 2021 First impurity powder injection experiments in LHD *Nucl. Mater. Energy* **25** 100842
- [22] Nespoli F. et al 2022 Observation of a reduced-turbulence regime with boron powder injection in a stellarator *Nat. Phys.* **18** 350–6
- [23] Wirth B. et al 2021 Measuring and modeling helium accumulation in single crystal tungsten specimens exposed to He plasma discharges in the WEST reciprocating collector probe 2020 IAEA Fusion Energy Conf. (Nice, France May 13th, 2021) EX/P5-3 (<https://conferences.iaea.org/event/214/contributions/17450/contribution.pdf>)
- [24] Meyer O. et al 2018 Visible spectroscopy diagnostics for tungsten source assessment in the WEST tokamak: first measurements *Rev. Sci. Instrum.* **89** 10D105

- [25] Gallo A. *et al* 2020 Interpretative transport modeling of the WEST boundary plasma: main plasma and light impurities *Nucl. Fusion* **60** 126048
- [26] Klepper C.C. *et al* 2020 W sources in the long-pulse, all-W wall, RF-heated WEST tokamak environment *47th European Physical Society Conf. Plasma Physics* (Sitges, Spain (Virtual) June 24th, 2021) (<http://ocs.ciemat.es/EPS2021ABS/pdf/I4.106.pdf>)
- [27] Urbanczyk G. *et al* 2021 RF wave coupling, plasma heating and characterization of induced plasma-material interactions in WEST L-mode discharges *Nucl. Fusion* **61** 086027
- [28] Philips J., Hodapp T., Holtrop K., Jackson G.L., Moyer R., Watkins J. and Winter J. 1992 Initial boronization of the DIII-D tokamak *J. Vac. Sci. Technol. A* **10** 1252
- [29] Behringer K., Summers H.P., Denne B., Forrest M. and Stamp M. 1989 Spectroscopic determination of impurity influx from localized surfaces *Plasma Phys. Control. Fusion* **31** 2059
- [30] Dejarnac R., Sestak D., Gunn J.P., Firdaouss M., Greuner H., Pascal J.-Y., Richou M. and Roche H. 2021 Flush-mounted Langmuir probes in the WEST tokamak divertor *Fusion Eng. Des.* **163** 112120
- [31] Johnson C.A., Loch S.D. and Ennis D.A. 2019 ColRadPy: a Python collisional radiative solver *Nucl. Mater. Energy* **20** 100579
- [32] Hill K.W. *et al* 1999 Tests of local transport theory and reduced wall impurity influx with highly radiative plasmas in the Tokamak fusion test reactor *Phys. Plasmas* **6** 877
- [33] McKee G., Burrell K., Fonck R., Jackson G., Murakami M., Staebler G., Thomas D. and West P. 2001 Impurity-induced suppression of core turbulence and transport in the DIII-D Tokamak *Phys. Rev. Lett.* **84** 1922
- [34] Maddison G.P. *et al* 2002 Impurity-seeded plasma experiments on JET *Nucl. Fusion* **43** 49
- [35] Unterberg B., Samm U., Tokar' M.Z., Messiaen A.M., Ongena J. and Jaspers R. 2005 The radiative improved mode in TEXTOR: power exhaust and improved confinement at high density *Fusion Sci. Technol.* **47** 187
- [36] Yang X. *et al* 2020 Core tungsten transport in WEST long pulse L-mode plasmas *Nucl. Fusion* **60** 086012
- [37] Artaud J.F. *et al* 2018 METIS: a fast integrated tokamak modelling tool for scenario design *Nucl. Fusion* **58** 105001
- [38] Bourdelle C., Citrin J., Baiocchi B., Casati A., Cottier P., Garbet X. and Imbeaux F. (JET Contributors) 2015 Core turbulent transport in tokamak plasmas: bridging theory and experiment with QuaLiKiz *Plasma Phys. Control. Fusion* **58** 014036
- [39] Maingi R. *et al* 2020 ELM suppression by boron powder injection and comparison with lithium powder injection on EAST *J. Fusion Energy* **39** 429